BRAIN
ORIGINAL ARTICLE

Single-nucleus transcriptomics reveals disease- and pathology-specific signatures in α-synucleinopathies

Gonzalo S. Nido,[1,2,3] Martina Castelli,[1] Sepideh Mostafavi,[1] Anna Rubiolo,[1,2,3] Omnia Shadad,[1,2] Guido Alves,[4,5] Ole-Bjørn Tysnes,[1,2] Irene H. Flønes,[1,2,3] Christian Dölle[1,2,3] and Charalampos Tzoulis[1,2,3]

α-Synucleinopathies are progressive neurodegenerative disorders characterized by intracellular aggregation of α-synuclein, but their molecular pathogenesis remains unknown. Here, we explore cell-specific changes in gene expression across different α-synucleinopathies. We perform single-nucleus RNA sequencing on nearly 300 000 nuclei from the prefrontal cortex of individuals with idiopathic Parkinson's disease (PD, $n = 20$), Parkinson's disease caused by *LRRK2* mutations (LRRK2-PD, $n = 7$), multiple system atrophy ($n = 6$) and healthy controls ($n = 13$).

Idiopathic PD and LRRK2-PD exhibit a largely overlapping cell type-specific signature, which is distinct from that of multiple system atrophy and includes an overall decrease of the transcriptional output in neurons. Notably, most of the differential expression signal in idiopathic PD and LRRK2-PD is concentrated in a specific deep cortical neuronal subtype expressing adrenoceptor alpha 2A. Although most differentially expressed genes are highly cell type and disease specific, *PDE10A* is found to be downregulated consistently in most cortical neurons and across all three diseases. Finally, exploiting the variable presence and/or severity of α-synuclein pathology in LRRK2-PD and idiopathic PD, we identify cell type-specific signatures associated with α-synuclein pathology, including a neuronal upregulation of *SNCA* itself, encoding α-synuclein.

Our findings provide new insights into the cell-specific transcriptional landscape of the α-synucleinopathy spectrum.

1 Neuro-SysMed, Department of Neurology, Haukeland University Hospital, 5021 Bergen, Norway
2 Department of Clinical Medicine, University of Bergen, 5020 Bergen, Norway
3 K.G. Jebsen Center for Translational Research in Parkinson's disease, University of Bergen, 5020 Bergen, Norway
4 The Norwegian Centre for Movement Disorders and Department of Neurology, Stavanger University Hospital, 4068 Stavanger, Norway
5 Department of Mathematics and Natural Sciences, University of Stavanger, 4062 Stavanger, Norway

Correspondence to: Charalampos Tzoulis
Neuro-SysMed Center of Excellence for Clinical Research in Neurological Diseases
Department of Neurology, Haukeland University Hospital
5021 Bergen, Norway
E-mail: charalampos.tzoulis@uib.no

Correspondence may also be addressed to: Gonzalo S. Nido
Neuro-SysMed Center of Excellence for Clinical Research in Neurological Diseases
Department of Clinical Medicine, University of Bergen

Received July 08, 2024. Revised October 05, 2024. Accepted October 14, 2024. Advance access publication November 15, 2024

5020 Bergen, Norway
E-mail: gonzalo.nido@uib.no

Keywords: Parkinson's disease; multiple system atrophy; *LRRK2*; single cell; nuclear transcriptomics; Lewy pathology

Introduction

α-Synucleinopathies are relentlessly progressive neurodegenerative disorders comprising Parkinson's disease (PD), dementia with Lewy bodies and multiple system atrophy (MSA).[1,2] These disorders share the common feature of intracellular α-synuclein-positive inclusions, which are generally believed to contribute to the neurodegenerative process.[3] In PD and dementia with Lewy bodies, α-synuclein inclusions occur mostly in neurons, assuming the form of Lewy bodies and neurites, collectively termed Lewy pathology, whereas in MSA they occur predominantly in the form of oligodendroglial cytoplasmic inclusions.[4,5] Although α-synuclein pathology is a hallmark of MSA, dementia with Lewy bodies and idiopathic PD (iPD), it is not always present in monogenic forms of PD, such as in patients with *LRRK2* mutations, about half of whom exhibit no Lewy pathology.[6,7] Currently, no disease-modifying therapies exist for α-synucleinopathies, with clinical trials yielding disappointing results largely owing to limited understanding of the molecular mechanisms underlying neuronal dysfunction and death.

Whole-genome transcriptomic studies in bulk brain tissue from individuals with α-synucleinopathies have shown low replicability, with findings largely driven by differences in cell composition (neuronal loss and gliosis), rather than disease-related changes within cells.[8-10] Single-nucleus RNA sequencing (snRNA-seq) addresses this limitation by enabling cell type-specific gene expression analysis. Previous snRNA-seq studies focused on the dopaminergic substantia nigra pars compacta in PD, providing valuable insights into the transcriptional state of individual cells.[11,12] However, an important drawback of studying substantia nigra pars compacta tissue is that it is typically degenerated severely in the terminal stage of the disease.[13] This complicates comparisons between cases and controls, because surviving dopaminergic neurons are difficult to isolate in sufficient numbers and are likely to represent resilient cells, introducing survival bias. In contrast, regions with milder involvement, such as the neocortex, might offer better insights into early disease processes.

Here, we used snRNA-seq to identify cell type proportions and cell type-specific gene expression signatures in the dorsolateral prefrontal cortex of individuals with iPD, monogenic PD caused by *LRRK2* mutations (LRRK2-PD) and MSA, in comparison to demographically matched controls. We find that the cell type-specific signatures of iPD and LRRK-PD are qualitatively similar and distinct from that of MSA, and we identify a large number of disease- and cell type-specific differentially expressed genes (DEGs). Furthermore, by comparing LRRK2-PD samples with and without α-synuclein pathology, we discern cell type-specific signatures of α-synuclein pathology.

Materials and methods

Sample cohort

Fresh-frozen dorsolateral prefrontal cortex (PFC) samples (Brodmann area 9) were obtained from 46 individuals: $n = 13$ healthy individuals, $n = 20$ idiopathic PD patients, $n = 7$ LRRK2-PDs ($n = 6$ p.G2019S and $n = 1$ p.R1441H) and $n = 6$ individuals with parkinsonian MSA. Brain samples were obtained from our brain bank for ageing and neurodegeneration, including samples from the Norwegian Park West cohort,[14] the Netherlands Brain Bank, the Barcelona Brain Bank and the London Neurodegenerative Diseases Brain Bank (Supplementary Table 1). Mean age (iPD = 79.4 years, LRRK2-PD = 79.0 years, MSA = 73.7 years and Control = 75.4 years) and hours of post-mortem interval (PMI) (iPD = 17.0, LRRK2-PD = 13.1, MSA = 14.7, Control = 25.2) did not differ significantly between groups (age: ANOVA $F = 0.84$, $P = 0.48$; PMI: ANOVA $F = 1.8$, $P = 0.16$). Likewise, sex was not significantly associated with the disease group (two-sided Fisher's test $P = 0.17$). Variant calling on the bulk RNA-seq samples was carried out by aligning the raw FASTQ files against the human reference genome assembly GRCh38 using HISAT2[15] v.2.2.1 and following the Broad Institute Best Practices for RNA-seq short variant discovery[16] (Supplementary material, 'Methods' section). Variant detection in transcribed regions revealed no known/predicted pathogenic mutations in genes implicated in Mendelian PD or other monogenic neurological disorders, with the exception of the LRRK2-PD samples, for which the expected variants could be confirmed. Owing to the intrinsic limitations of short-read sequencing, *GBA* mutations in the pseudogene homology region could not be excluded confidently. Controls had no known neurological disease. Individuals with PD fulfilled the National Institute of Neurological Disorders and Stroke[17] and the UK Parkinson's Disease Society Brain Bank[18] diagnostic criteria for the disease at their final visit. Informed consent was available from all individuals.

Isolation of single nuclei, single-nucleus RNA-seq library preparation and sequencing

Because of the complex morphology of brain cells and the inherent difficulty in dissociating them without causing severe damage, single-cell transcriptomics of human post-mortem brain are generally restricted to the use of nuclei. The procedure for isolation of nuclei was performed as described,[19] with minor modifications. Methodological details are provided in the Supplementary material, 'Methods' section.

A total of 10 000 nuclei per sample were targeted for droplet-based snRNA-seq. Complementary DNA synthesis and DNA library preparation were carried out using the Chromium Next GEM Single Cell 3′ Reagent Kit v.3.1 Dual Index (10x Genomics) according to the manufacturer's protocol. DNA libraries were pooled and run using paired-end (300 million read pairs per sample) sequencing on the NovaSeq 6000 platform (Illumina) at Novogene (Cambridge).

Bulk tissue RNA-seq library preparation and sequencing

Total RNA was extracted from PFC tissue homogenate for all samples using the RNeasy plus mini kit (Qiagen) with on-column DNase treatment according to the manufacturer's protocol.

Library preparation was carried out using Ribo-Zero™ Gold (Epidemiology) kit (Illumina) using the manufacturer's recommended protocol. Two samples did not pass quality control and were not sequenced (Supplementary Table 1). Further details are provided in the Supplementary material, 'Methods' section. Paired-end sequencing of 125 bp was performed on an Illumina HiSeq2500 sequencer (Illumina).

Single-nucleus RNA-seq analyses

The snRNA-seq raw FASTQ files were aligned to the human genome (GRCh38) using CellRanger v.6.1.2 (10x Genomics) also accounting for intronic reads to include all nuclear transcripts (include-introns option) and excluding secondary mappings ('nosecondary' option). To estimate the intronic:exonic ratio, an additional alignment was carried out, only accounting for reads mapped to exonic reads. Version 35 of the ENCODE transcriptome assembly (Ensembl 101) was used. ANOVA tests revealed no significant associations between sequencing quality control metrics (i.e. number of raw reads, per cent of reads with mapping quality above 20, per cent of reads with mapping quality above 30 and per cent of GC content) and the disease status. The same was the case for each of the quality control metrics provided by CellRanger (Supplementary material, 'Data' section 1).

Non-nuclear ambient RNA and empty droplets were initially discarded using CellBender.[20,21] In a first filtering pass, droplets with <500 features, <1000 counts, >3% mitochondrial reads or >2% ribosomal reads were discarded. Doublets were estimated using doubletFinder[22] and barcodes clustered using a low resolution with Seurat to discard non-nuclear clusters. Barcodes were filtered out if they fulfilled any of the following conditions: (i) above the 90th percentile in Unique Molecular Identifier (UMI) counts; (ii) above the 90th percentile in number of genes; and (iii) identified as a doublet. The resulting dataset was then reclustered for a second filtering pass using a higher resolution. Expression of known cell type markers was used for cluster annotation, allowing a straightforward identification of additional clusters composed of doublets and undefined populations of cells. The resulting 28 final clusters (12 clusters of excitatory neurons, eight of inhibitory neurons, three of oligodendrocytes, two of astrocytes, one microglial cluster, one oligodendrocyte precursor cell cluster and one endothelial cluster) were trimmed by removing barcodes that had zero UMI counts for either of the two respective major cell type markers, resulting in a final dataset of 299 582 barcodes (121 701 excitatory neurons, 44 711 inhibitory neurons, 83 302 oligodendrocytes, 26 178 astrocytes, 14 755 oligodendrocyte precursor cells, 6897 microglia and 2038 endothelial nuclei; Fig. 1). Subclusters of neurons were classified based on markers described previously[24] (Fig. 1E and F, Supplementary Fig. 1 and Supplementary material, 'Methods' section).

Bulk tissue RNA-seq analyses

Bulk RNA-seq was carried out for neighbouring tissues from the same individuals. A total of 44 of 46 samples succeeded library preparation (two control samples failed quality control; Supplementary Table 1). We used Salmon[25] v.1.3.0 to quantify the abundance at the transcript level with the fragment-level GC bias correction option (gcBias) and the appropriate option for the library type (ISR) against the GENCODE annotation release 35. Transcript-level quantification was collapsed onto gene-level quantification using the tximport[26] R package v.1.28.0. We restricted the analyses to protein-coding genes in autosomal chromosomes.

Cell type quantification

Cell type quantification was carried out using marker gene profiles (MGPs).[27] MGPs are based on the across-sample relative expression of cell type markers, estimating cellularity from a volumetric perspective (i.e. proportion of the transcriptomic library originating from each cell type) rather than estimating the number of cells (i.e. the number of nuclei). The MGP estimates are thus influenced by a combination of relative cell type abundance (i.e. number of cells) and relative cell type-specific transcriptional output (i.e. cell types with more RNA content will result in larger estimates). MGPs were calculated independently for the bulk RNA-seq expression and for the snRNA-seq pseudobulk expression (per-sample aggregated reads of all filtered barcodes). Additionally, we considered the proportion of nuclei labelled in the snRNA-seq dataset to each major cortical cell type as an alternative cell type estimate. Prior to the calculation of MGPs, count data were normalized using a variance-stabilizing transformation (*vst* function from the DESeq2[28] R package v.1.40.2). MGPs were calculated using the cortical markers from the NeuroEspresso database,[27] with human orthologues defined using the Homologene[29] R package v.1.4.68 as previously described.[8]

To assess differences in cortical cell type proportions between diseases and controls, we used a linear regression for the MGP-based estimates accounting for age, sex, PMI and disease status. For the estimates based on the number of nuclei, counts were modelled using a generalized linear regression using a negative binomial distribution accounting for age, sex and PMI.

Analysis of the effect of demographic variables in the cortical transcriptome

We correlated demographic variables (age, sex and PMI) with MGP-based cell type estimates in the bulk RNA-seq samples to reveal that age and PMI were strongly associated with the MGP-based cell type estimates (Supplementary Fig. 2). In particular, longer PMIs were associated with a relative decrease in the neuronal signal, in agreement with previous observations.[30] To characterize these sources of variation further, we modelled: (i) the number of detected genes per droplet; and (ii) the proportion of nuclei in the snRNA-seq dataset as a function of the demographic variables independently for each of the 28 cell type clusters. Age, sex, PMI and diagnosis were modelled as fixed effects, with individual as a random intercept. As expected, we observed a strong, consistent decrease in the transcriptional volume with longer PMIs in all neuronal clusters, a trend that was absent in glial cells (Supplementary Fig. 3A). The proportion of captured neuronal nuclei, however, did not show a consistent variation across neuronal subtypes (Supplementary Fig. 3B). Age was, if anything, positively associated with transcriptional output, although only in some clusters and with no marked differences between neuronal and glial populations. These results highlighted the importance of controlling for demographic covariates in downstream analyses.

To test for a relative decrease in the transcriptional volume in neurons, we used the number of detected genes per droplet as a proxy. We defined three major clusters (excitatory neurons, inhibitory neurons and glia) and modelled the number of genes per droplet as a function of age, sex, PMI, disease status and major cluster, adding an interaction term for Disease status × Major cluster and accounting for differences between cell type clusters (nested within the major clusters) with a random intercept, while the cell type-specific effect of PMI was accounted for with a random slope and

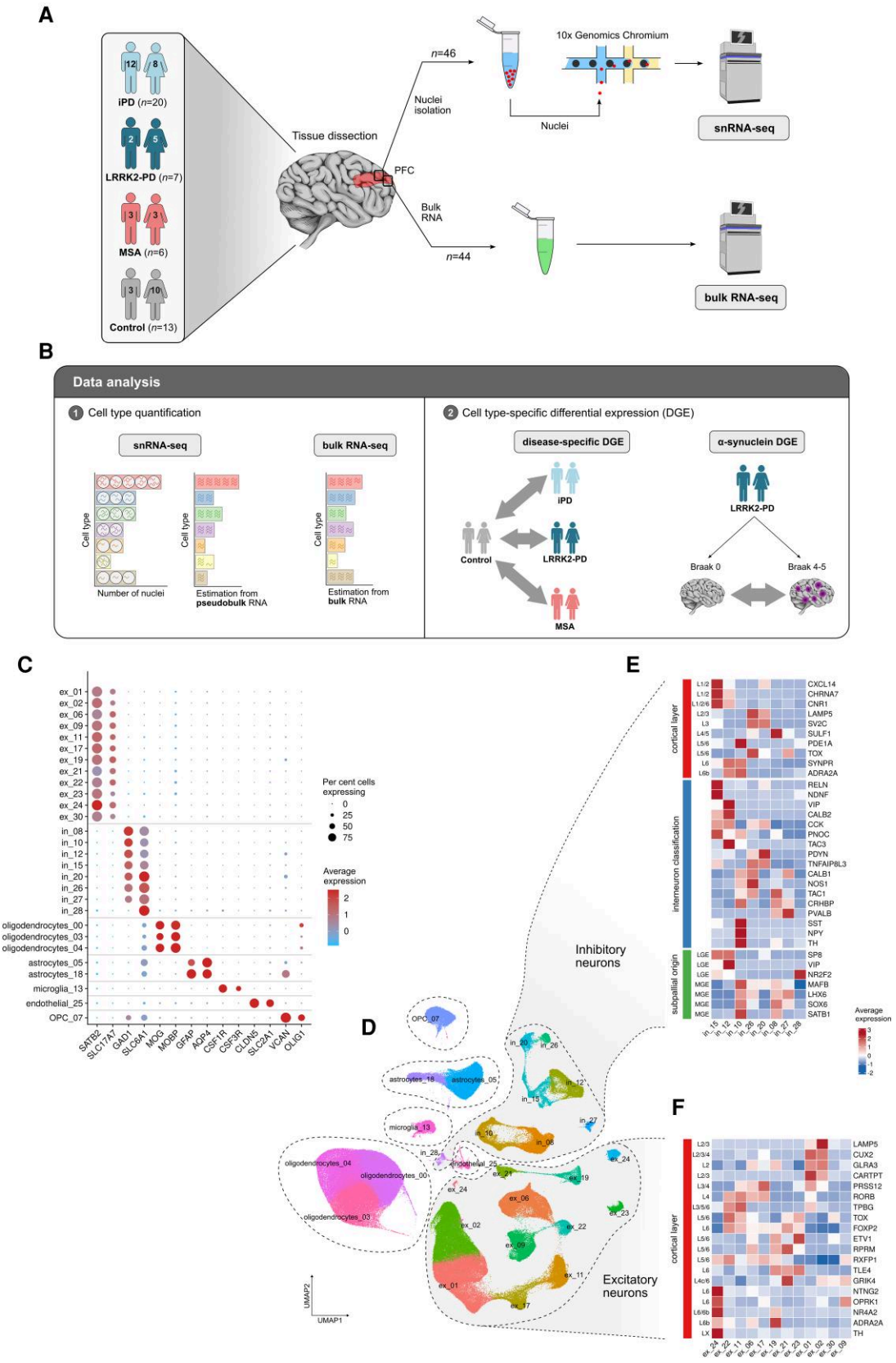

Figure 1 Single-nucleus transcriptomics in α-synucleinopathies. (**A**) Experimental workflow for tissue processing. Two adjacent tissue samples from fresh frozen prefrontal cortex (PFC, Brodmann area 9) were obtained from 46 individuals. Suspensions of nuclei were processed using the 10x Genomics Chromium platform and subsequently underwent deep RNA sequencing (snRNA-seq). RNA -sequencing was also conducted in bulk tissue samples (bulk RNA-seq). (**B**) Both snRNA-seq and bulk RNA-seq datasets were assessed for cell type composition and differential gene expression (DGE). Cell type

(Continued)

intercept. Age and PMI were scaled and centred, whereas the other categorical variables were modelled as dummy variables.

Differential gene expression

Differential gene expression analysis in the snRNA-seq dataset between each diagnosis (iPD, LRRK2-PD and MSA) and controls was carried out independently for each cluster using the MAST R package[31] v.1.24.1. The regressions were limited to the genes with UMI counts > 0 in 25% of the barcodes in the cluster. Sex, age, PMI and the proportion of genes detected in each droplet were modelled as fixed effects, with individual as a random effect (Supplementary Fig. 1). To account for the interaction between demographic variables and cell type identity (Supplementary Fig. 4), differential gene expression analyses were carried out independently for each cell type cluster. The *P*-values were corrected for multiple testing using the Benjamini–Hochberg false discovery rate (FDR) for each cluster.

To characterize the transcriptional signature associated with brain α-synuclein deposition, we first carried out differential gene expression analysis between the LRRK2-PD samples without α-synuclein deposition (Braak stage 0; $n = 4$) and the LRRK2-PD samples with Braak stages 4–5 ($n = 3$). In addition, we carried out an independent differential gene expression analysis using only iPD samples, with Braak stages ranging from 4 to 6.

The subset of genome-wide association study-nominated genes was initially obtained from Nalls *et al.*,[32] and non-protein-coding transcripts were filtered out, resulting in 91 genes.

Differential gene expression analysis of bulk RNA-seq was performed using the DESeq2 R package[28] v.1.40.2 with default parameters and as previously described.[8]

Gene set enrichment analyses

To test for enrichment of functional terms within the lists of DEGs, we ran overrepresentation analyses using the *fora()* function from the R fgsea package[33] v.1.26 with the entire Gene Ontology (GO) database obtained from the enrichR database[34] and the Hallmark dataset from the MSigDB database[35,36] v.2024.1.Hs. For a given cell type cluster, we used the nominally significant genes as input and the expressed genes in the cluster as background to minimize trivial enrichment in cell type markers. Overrepresentation analyses were carried out independently for up- and downregulated genes (directional) and using up- and downregulated genes combined (non-directional). When a list of DEGs consisted of the intersection between two contrasts, the overlapping input gene lists were restricted to DEGs from the same cell type clusters and with concordant directions of change. Multiple testing correction was calculated using Benjamini–Hochberg FDR.

Immunohistochemistry and image analyses

Immunohistochemistry was performed on 3.5-µm-thick formalin-fixed, paraffin-embedded PFC sections from 14 individuals (iPD, $n = 7$; controls, $n = 7$). Deparaffinization and antigen retrieval were performed in low pH EnVision FLEX Target Retrieval Solution at 98°C for 24 min in the DAKO PT link from Agilent. Sections were rinsed with TBS Automation Wash buffer (Biocare, TWB945M) and blocked with hydrogen peroxide (Peroxidased 1, Biocare, PX968M) for 10 min. After 5 min washing in TBS, sections were incubated in a humidified chamber for 1 h at room temperature with rabbit anti-PDE10A (Abcam, ab151454) diluted 1:1000 in Da Vinci Green Diluent (Biocare, PD900M). Sections were washed for 5 min in TBS, then incubated with HRP-Polymer (Biocare, MRH534L) for 30 min. After two rounds of 5 min washing in TBS, DAB chromogen (Biocare, DB801) was applied for 4 min. After the visualization step, sections were washed in tap water for 30 s, counterstained with Tachas's Haematoxylin (Biocare, NM-HEM-M) for 3 min, and washed again in tap water for 5 min. Finally, sections were dehydrated by immersion in a series of graded alcohol solutions (from 75% ethanol to 100% ethanol) and xylene and covered with glass coverslips using Pertex mounting medium (Histolab, 00811).

Slides were digitally scanned using the NanoZoomer XR (Hamamatsu). Neuronal staining intensity was assessed visually, using the NDP.view2plus v.2.7.25 software (Hamamatsu), using a scale of 0–3, with 0 indicating a lack of staining and 3 indicating an intense dark brown staining. Each section was assessed by two independent raters, blinded to the disease group. Interrater reliability was tested using Cronbach's α coefficient, and the mean value was used in downstream analyses. Normality was tested using the Shapiro–Wilk test, and homogeneity of variances was tested using Levene's test. Statistical group comparison was performed using a two-sided *t*-test.

Results

Single-nucleus RNA-seq profiling of the prefrontal cortex in α-synucleinopathies

We isolated nuclei from the dorsolateral PFC of individuals with iPD ($n = 20$), LRRK2-PD ($n = 7$), parkinsonian-type MSA ($n = 6$) and demographically matched neurologically healthy controls ($n = 13$; Fig. 1A and Supplementary Table 1). We obtained snRNA-seq data from 299 582 high-quality nuclei. Integration of the complete dataset evidenced clusters for the main cortical cell types, identified by their respective marker expression levels (Fig. 1C). High-resolution clustering revealed a total of 28 subclusters (Fig. 1D). Neuronal subclusters were characterized further by cortical neuronal markers (Fig. 1E and F). Bulk RNA-seq data were obtained from immediately adjacent cortical samples from the same individuals, except for two control samples that failed quality control (Supplementary Table 1).

Cortical neurons show lower transcriptional output in α-synucleinopathies

Cell type composition was assessed by multiple methods in bulk RNA-seq and snRNA-seq data from the same individuals. Bulk

Figure 1 Continued
composition was estimated in the snRNA-seq dataset by two alternative approaches, based on the nuclei counts, or marker gene profiles[14] (MGPs) on the pseudobulk data (see the 'Materials and methods' section). The MGPs were also used to estimate cell types in the bulk RNA-seq samples. Differential gene expression was calculated for each disease group [i.e. control versus idiopathic Parkinson's disease (iPD), control versus PD caused by LRRK2 mutations (LRRK2-PD) and control versus multiple system atrophy (MSA)] and for Lewy pathology Braak stage 0 versus Braak stage 4–5 within the subset of LRRK2-PD samples. Grey arrows indicate the contrasts. (**C**) Dot plot of average gene expression in subclusters of cell type markers for the main cortical cell types. (**D**) UMAP embeddings for the snRNA-seq dataset. Colours correspond to different clusters identified by Seurat at a resolution of 0.5. Dashed contours are drawn to aid visualization of the clusters corresponding to the main cortical cell types [12 clusters of excitatory neurons, eight inhibitory neurons, three oligodendrocytes, two astrocytes, microglia, oligodendrocyte precursor cells (OPCs) and endothelial cells]. (**E**) Heat map of average expression of markers for excitatory neurons. Left annotation labels indicate cortical layer (*top*), interneuron classification (*middle*) and subpallial origin (*bottom*), as proposed by Lake *et al.*[24] (**F**) Heat map of average expression of markers for inhibitory cortical neurons. Labels on the *left* indicate the cortical layer location of the markers.

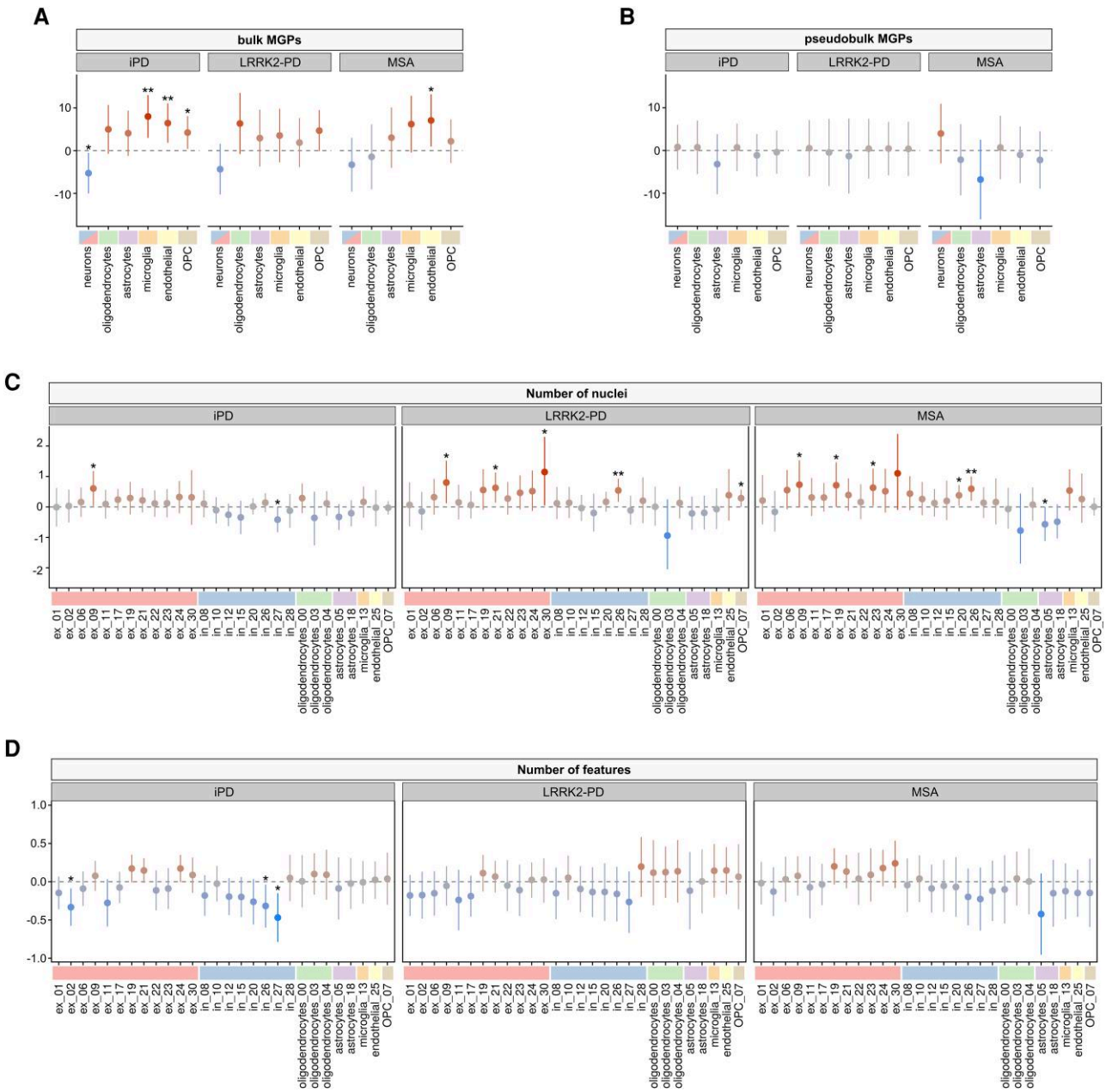

Figure 2 Cell type composition. Changes in relative cell type abundance are displayed as average fold-change in the disease compared with control samples. (**A**) Marker gene profile (MGP)-based estimates calculated in bulk RNA-seq samples for the major cortical cell types showed a decrease in the relative abundance of neuronal transcripts and an increase in glial transcripts consistent with previous results. (**B**) MGP-based estimates calculated in pseudobulk tissue from the snRNA-seq samples (i.e. from a highly enriched nuclear fraction) of the major cortical cell types. Here, the cell type estimates did not exhibit significant deviations between cases and controls. (**C**) Changes in the proportions of captured nuclei in the snRNA-seq dataset for all cell type clusters. Similar to the pseudobulk results, the proportion of nuclei for the different cell types did not seem to follow the established notion of neuronal loss accompanied by gliosis, as observed in the bulk tissue transcriptome. On the contrary, nuclei of excitatory neurons appear overrepresented in the diseases. (**D**) Log fold-changes in the number of features (genes) detected per barcode show a mild but consistent decrease in the transcriptional output of most neuronal clusters in comparison to the glial populations in both idiopathic Parkinson's disease (iPD) and PD caused by LRRK2 mutations (LRRK2-PD). Coefficients were estimated as follows: for **A** and **B** (fold-changes), with a linear regression; for **C** (log fold-changes), using a negative binomial regression with (log) total number of nuclei as offset; and for **D** (log fold-changes), using a linear mixed model with sample as random effect. For all models, sex, age and post-mortem interval (PMI) were accounted for in the fit. Vertical bars: 95% confidence interval. MSA = multiple system atrophy.

RNA-seq data exhibited a relative decrease in neurons and increase in glia in all three diseases, with the single exception of decreased oligodendrocytes in MSA (Fig. 2A). Pseudobulk analyses of the snRNA-seq data did not recapitulate these differences, revealing no differences in the relative abundances of cell types (Fig. 2B). Furthermore, the proportions of cell types based on the number of captured nuclei showed no major differences across the 28 identified cell types. In fact, most neuronal clusters exhibited a mild trend for increase in iPD, LRRK2-PD and MSA compared with controls, although this only reached nominal significance for few clusters (Fig. 2C).

Although there is evidence of bias towards certain cell type populations during isolation of nuclei,[37] it is unlikely that this would be disease specific. Therefore, we reasoned that the observed disease-specific decrease in neuronal signal in the bulk RNA-seq

data could be explained by: (i) a decrease in the extranuclear fraction of the transcriptome of neurons (i.e. loss of cytoplasmic and/or synaptic transcripts); and/or (ii) a decrease in the neuronal transcriptional output per neuron (i.e. an overall decrease in the number of nuclear transcripts per cell). To explore this question, we compared the number of genes per captured nucleus between each of the three disease groups and controls, per cell type. This analysis indicated a general trend for decrease in the total number of expressed genes in 14 of 20 neuronal clusters in iPD and 14 of 20 in LRRK2-PD. Conversely, a trend for increase in the number of expressed genes was seen in five of eight glial clusters in iPD and seven of eight in LRRK2-PD (Fig. 2D). This trend was not observed in MSA. To test formally whether the number of expressed genes in neurons and glia was indeed altered in disease, we combined nuclei into three major clusters (excitatory neurons, inhibitory neurons and glia). iPD and LRRK2-PD exhibited a significant decrease in the number of expressed genes in both inhibitory and excitatory neurons, relative to glia, with the largest decrease exhibited in iPD. MSA exhibited only mild changes, which did not reach statistical significance (Supplementary Table 2).

Parkinson's disease and multiple system atrophy show distinct cell-specific expression profiles

For each of the 28 cell type clusters, we calculated differential gene expression between each disease group and controls. We found a total of 272 DEGs in iPD, 54 in LRRK2-PD and 125 in MSA, at FDR < 5% (Supplementary material, 'Data' sections 2–4).

iPD and LRRK2-PD exhibited predominantly a downregulation signal in excitatory neurons (iPD, 31 upregulated and 115 downregulated DEGs; LRRK2-PD, 11 upregulated and 23 downregulated DEGs) and inhibitory neurons (iPD, 10 upregulated and 23 downregulated DEGs; LRRK2-PD, one upregulated and three downregulated DEGs; Fig. 3A and B). The neuronal signature in iPD and LRRK2-PD was qualitatively similar, with 60% (23 of 38) of LRRK2-PD DEGs found also in the iPD group, in contrast to only 10% (4 of 38) of LRRK2-PD DEGs present in MSA (Fig. 3G). The excitatory cluster ex_19 stood out in both idiopathic and monogenic forms of PD as the most affected cell type in the cortex (Fig. 3A and B). The marker expression profile places ex_19 in the deep cortical layers (layer 6/layer 6b), characterized by the highest relative expression of *ADRA2A*, encoding the α_{2A}-adrenoreceptor, across all excitatory subtypes (Fig. 1E). Thus, these neurons appear to have a high density of adrenergic afferents.

MSA showed a highly distinct transcriptional signature in comparison to iPD and LRRK2-PD. It exhibited a predominant upregulation of gene expression in excitatory neurons (42 upregulated and 17 downregulated DEGs), which was particularly evident in the most abundant excitatory subtypes of the outermost cortical layers (ex_01 and ex_02, layers 2/3; Fig. 1E), but also manifest in ex_09, located deeper in the cortex. Contrarily to both PD groups, MSA did not display a pronounced dysregulation of the ex_19 neuronal subtypes (Fig. 3C) and had a low concordance in neuronal DEGs with both iPD and LRRK2-PD (19% (13 of 69) of MSA DEGs found in iPD and 6% (4 of 69) present in LRRK2-PD; Fig. 3G).

PDE10A is downregulated in most PFC neurons in Parkinson's disease, LRRK2-PD and multiple system atrophy

Most DEGs were highly cell type specific, i.e. 81% (255 of 313) were unique to a cell type cluster. The remaining 19% of the DEGs occurred in two to five cell types, with a single striking exception: *PDE10A* was found to be significantly downregulated in 14 clusters, comprising 10 of 12 excitatory neuronal types and four of eight inhibitory neuronal types in iPD. Moreover, although *PDE10A* was significantly downregulated in only a single neuronal cluster in LRRK2-PD, it was consistently downregulated at the nominal level (uncorrected $P < 0.05$) in the majority of neuronal clusters in both LRRK2-PD (15 of 20 neuronal clusters) and MSA (12 of 20 neuronal clusters; Fig. 3D–F). *PDE10A* encodes phosphodiesterase 10A, a protein known to be highly expressed in the human striatum.[38] Our data showed that *PDE10A* is abundantly expressed in all neuronal cell types and in endothelial cells of the human PFC, whereas its expression in glial cells is low (Fig. 4A).

To validate these findings at the protein level, we performed immunostaining on formalin-fixed, paraffin-embedded sections of PFC from iPD patients ($n = 7$) and controls ($n = 7$). In line with the snRNA-seq data, the staining revealed a strong cytoplasmic expression of the PDE10A in PFC neurons and in endothelial cells (Fig. 4C–E). Evaluation of the sections by two independent investigators who had been blinded to the disease group revealed a significantly weaker neuronal staining intensity in PD compared with controls (staining intensity score 0–3; iPD, 1.75 ± 0.59; controls, 2.57 ± 0.13; two-sided *t*-test: $P = 0.009$) with high interrater reliability (Cronbach's $\alpha = 0.87$; Fig. 4B).

Disease-specific dysregulation of glial gene expression

Dysregulation of gene expression was also found within glial populations. Oligodendrocytes presented dysregulated expression in nine genes in iPD (*ENOSF1*, *POLR2F*, *FOLH1*, *CD22*, *PCM1*, *SEMA3C*, *SPP1*, *NXX6-2* and *SELENOP*), two in LRRK2-PD (*FBXL17* and *SEMA3C*) and eight in MSA (*AK5*, *SIK3*, *LPAR1*, *UNC5C*, *FUT8*, *EPM2AIP1*, *MAT2A* and *OSBPL1A*). Except for *SEMA3C*, which was upregulated in the oligodendrocytes_04 cluster in both iPD and LRRK2-PD, no DEGs overlapped between groups (Fig. 5). In addition, MSA showed a significantly altered expression in three genes within the two astrocytic populations (*RAPGEF3*, *ABHD3* and *BNIP3L*), whereas no DEGs were found in the two PD forms. Of note, *BNIP3L* was consistently downregulated in all glial subtypes in MSA, albeit only nominally significant ($P < 0.05$). In the microglial population, a single DEG was detected in MSA (*RNASET2*) and two in the oligodendrocyte precursor cell cluster (*MAPT* and *CHST9*), whereas the two PD forms reported no significant differences in expression within these glial clusters. Finally, endothelial cells showed a single DEG for iPD (*DDX58*) and for LRRK2-PD (*COL4A2*) and two for MSA (*DDX60L* and *SLCO2B1*; Fig. 5).

Pathway enrichment analysis highlights dysregulation of ribosomal pathways

Functional enrichment in DEGs was carried out by overrepresentation analysis of GO pathways and the Hallmark dataset. The upregulated DEGs identified in iPD in the ex_19 and ex_21 clusters showed a significant enrichment in functions associated with protein translation, mostly attributable to the collective upregulation of ribosomal and associated transcripts. The same ribosomal-enriched signature was found in LRRK2-PD, albeit restricted to the ex_19 cluster, with the functional relevance of protein synthesis highlighted further by numerous non-ribosomal proteins ('RNA binding' GO term). In addition, iPD ex_19 was enriched in the GO term 'MHC Class II Protein Complex Binding', with three of six upregulated genes being heat shock protein transcripts

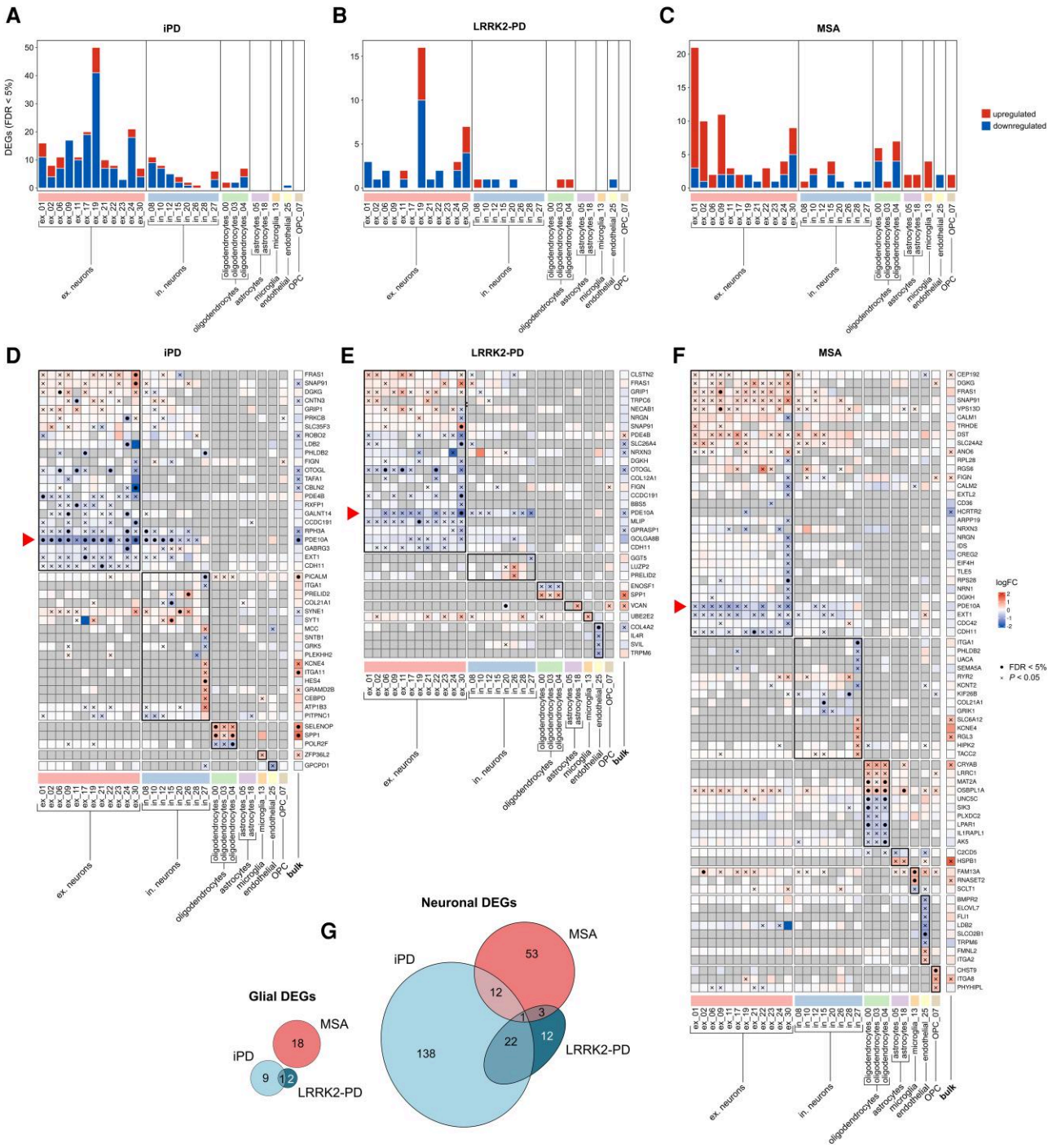

Figure 3 Differential gene expression within cell type clusters. (**A**–**C**) Number of differentially expressed genes (DEGs) at a false discovery rate (FDR) < 5% in each cell type cluster. Each panel corresponds to the contrast between the disease [**A**, idiopathic Parkinson's disease (iPD); **B**, PD caused by LRRK2 mutations (LRRK2-PD); **C**, multiple systems atrophy (MSA)] and the healthy controls. (**D**–**F**) Heat maps representing log fold-change in expression between diseases and controls in each cell type cluster (*columns*). Genes (*rows*) are represented in the heat maps only if they exhibit a log2 fold-change (logFC) below −0.5 or above 0.5 in at least one cluster. Nominal significance ($P < 0.05$) is represented by multiplication symbols; DEGs (FDR < 5%) are represented with black dots. Red arrowheads highlight the row corresponding to *PDE10A*. (**G**) Venn diagrams with neuronal and glial DEGs in the three diseases. Overlaps between contrasts represent common DEGs with concordant direction of change.

(*HSP90AA1*, *HSPA8* and *HSP90AB1*). Other overrepresented terms in upregulated DEGs in iPD were 'Vesicle' (also in ex_19), 'Calcium ion transmembrane import into cytosol' (in_27) and 'Establishment of mitotic sister chromatid cohesion', with the five components of the cohesin complex upregulated in ex_06 (Supplementary Table 3 and Supplementary material, 'Data' section 5).

In contrast to PD, MSA exhibited a downregulation of ribosomal pathways. This was observed in neuronal cluster ex_30, which also showed a significant downregulation of nuclear encoded OXPHOS subunits. Additional overrepresented GO terms in MSA included 'Microtubule binding' (upregulation in ex_01 and ex_06), 'Mitotic spindle' (upregulation in ex_09) and 'GTPase binding' (upregulation

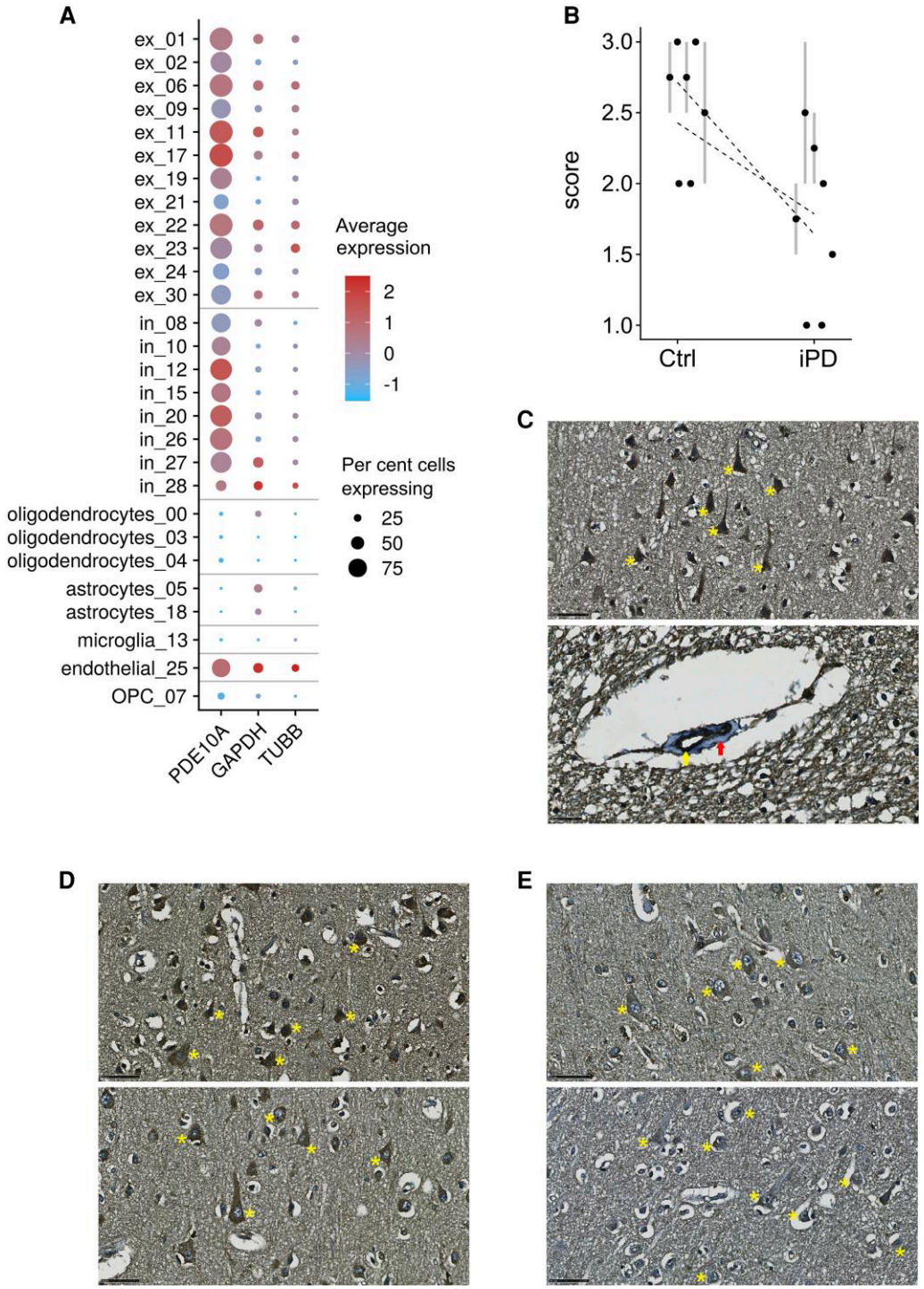

Figure 4 Expression of *PDE10A* in the prefrontal cortex. (**A**) Dot plot shows the relative expression of the *PDE10A* transcript in each cell type cluster for the complete snRNA-seq dataset. Housekeeping genes *GAPDH* and *TUBB* are shown as a reference. (**B**) Quantification of immunohistochemistry images in idiopathic Parkinson's disease (iPD, $n = 7$) and controls ($n = 7$). The plot represents the mean score values (staining intensity scored from 0–3) between the two raters (black points), with grey bars spanning between the individual values of each rater when not in agreement (iPD, 1.75 ± 0.59; controls, 2.57 ± 0.13; two-sided *t*-test, $P = 0.009$). Dashed lines indicate linear regression for the scores for each rater. (**C–E**) Immunohistochemistry images for PDE10A. (**C**) PDE10A is highly expressed in neurons (*top panel*) and endothelial cells (*bottom panel*). Examples of neurons are indicated by asterisks. The *left* and *right* arrows indicate the endothelial layer and muscle layer of the vessel, respectively. *Top*: Magnification ×500; scale bar = 50 μm. *Bottom*: Magnification ×800; scale bar = 25 μm. (**D** and **E**) Representative sections stained for PDE10A are shown from two controls (**D**) and two individuals with iPD (**E**). Examples of neurons are indicated by asterisks. Magnification ×500; scale bar = 50 μm.

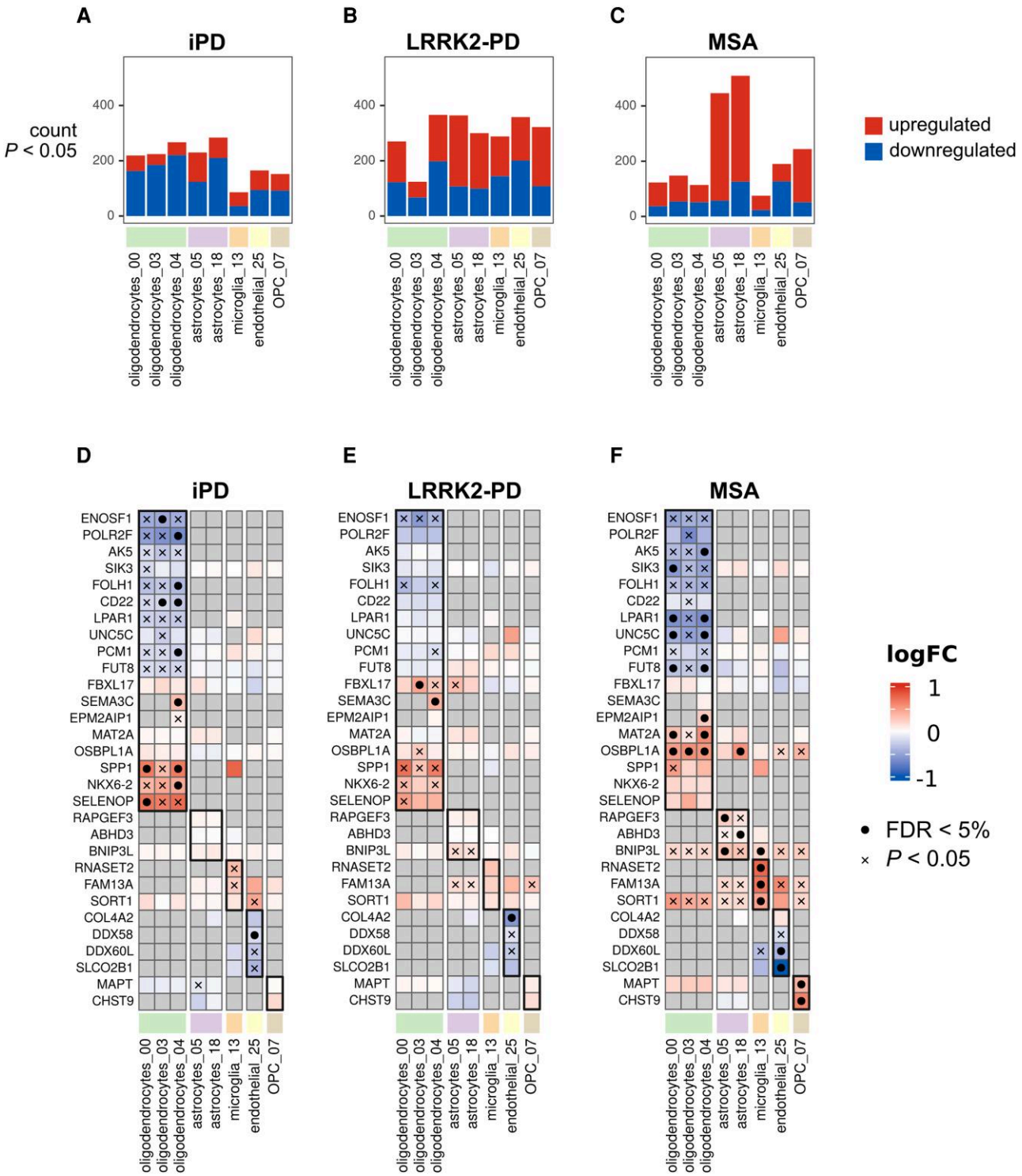

Figure 5 Differential gene expression within glial cell type clusters. (**A–C**) Number of differentially expressed genes (DEGs) at nominal $P < 0.05$ in each glial cell type cluster between disease groups and healthy controls. (**D–F**) Heat maps represent log fold-change (logFC) in expression between diseases and controls in each glial cell type cluster (columns). Genes (rows) are represented in the heat maps only if they are significantly expressed [false discovery rate (FDR) < 5%] in at least one cell type cluster in at least one group. Black dots indicate statistical significance at FDR < 5%; the multiplication symbols represent significance at the nominal level ($P < 0.05$). iPD = idiopathic Parkinson's disease; LRRK2-PD = PD caused by LRRK2 mutations; MSA = multiple systems atrophy.

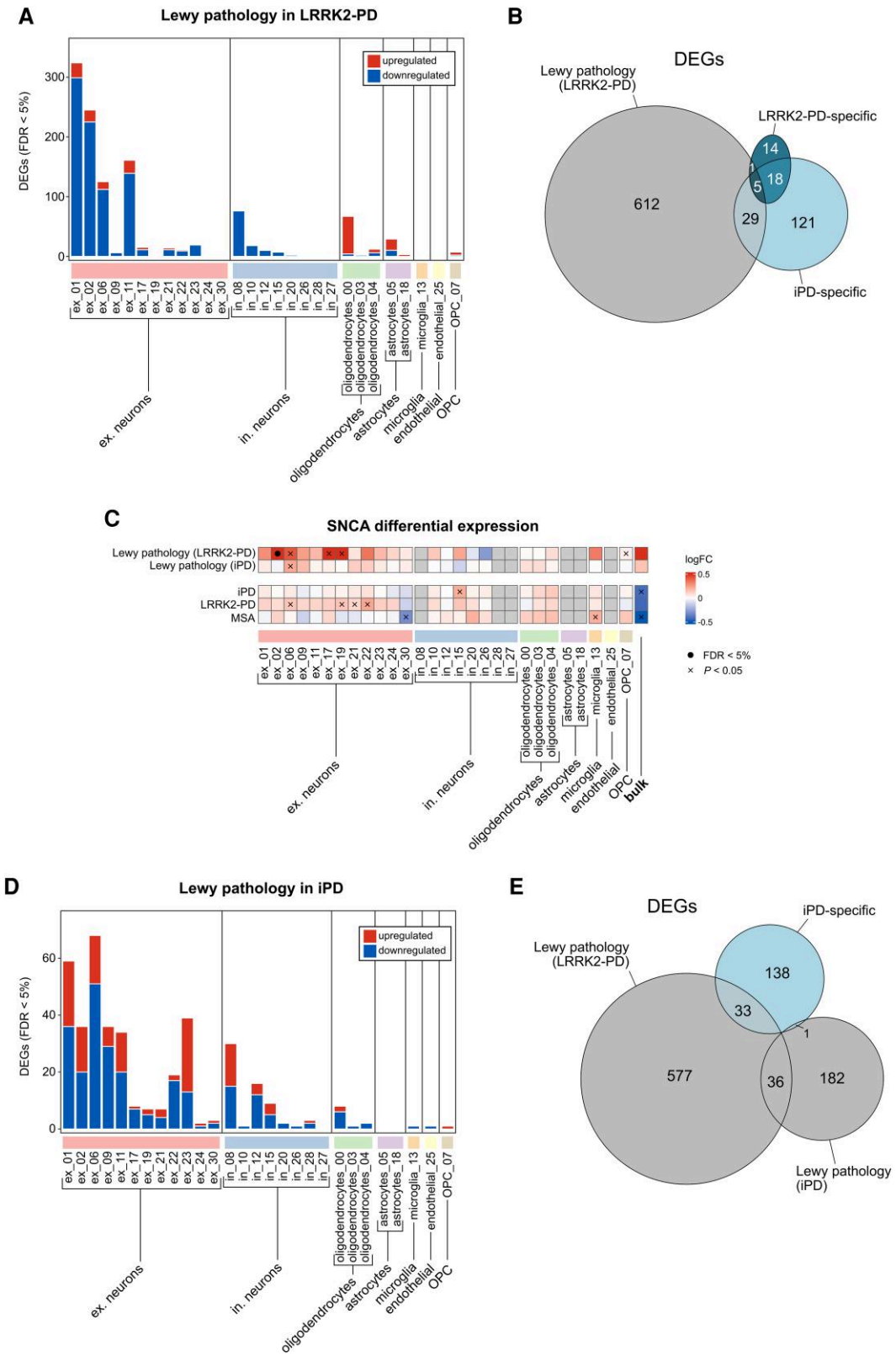

Figure 6 Differential gene expression associated with Lewy body pathology. (**A**) Number of differentially expressed genes (DEGs) at a false discovery rate (FDR) < 5% in each cell type cluster between LRRK2-PD samples derived from brains without α-synuclein pathology (Braak 0) and LRRK2-PD samples from brains with α-synuclein pathology (Braak 4–5). (**B**) Venn diagram showing overlap between neuronal DEGs in α-synuclein pathology in LRRK2-PD samples and disease-specific neuronal DEGs for idiopathic Parkinson's disease (iPD) versus controls and LRRK2-PD versus controls. (**C**) Heat map representing log fold-change (logFC) in expression of *SNCA* associated with α-synuclein pathology (within LRRK2-PD patients, *top row*; within iPD patients, *second row*) and between diseases and controls (*three bottom rows*). Grey tiles correspond to expression levels below prefiltering threshold in the cell type cluster. Black dots indicate FDR < 5%; crosses indicate nominal significance ($P < 0.05$). (**D**) Number of DEGs associated with the degree of α-synuclein pathology in iPD samples (Braak range 4–6). (**E**) Venn diagram showing overlap in neuronal DEGs associated with Lewy pathology in LRRK2-PD samples, neuronal DEGs associated with Lewy pathology in iPD samples and neuronal DEGs between iPD and controls. LRRK2-PD = Parkinson's disease caused by LRRK2 mutations; MSA = multiple systems atrophy; OPC = oligodendrocyte precursor cell.

in ex_02; Supplementary Table 3 and Supplementary material, 'Data' section 5).

Glial clusters did not exhibit significant functional overrepresentation in any of the α-synucleinopathies. Endothelial cells showed a significant downregulation of the interferon alpha and gamma response functions in iPD, which also appeared in LRRK2-PD, although only at the nominal level.

Cell type-specific differential expression of genes with a known association with Parkinson's disease

A total of 69 of 91 PD genome-wide association study-nominated protein-coding genes[32] were detected in at least one cell type cluster. Among these, *VPS13C*, *IGSF9B* and *KCNIP3* were differentially expressed in iPD (FDR < 5%), each in one excitatory neuron cluster (ex_21, ex_19 and ex_09, respectively). Notably, *VPS13C* was overexpressed at a nominal level ($P < 0.05$) in all excitatory clusters except for ex_17 (Supplementary Fig. 4). In LRRK2-PD, no genome-wide association study-nominated genes were among the DEGs (Supplementary Fig. 4). None of the known genes causing familial monogenic PD (*LRRK2*, *VPS35*, *PINK1*, *PINK7*, *PRKN* and *SNCA*) was differentially expressed in any of the PD forms (Supplementary Fig. 4). Overrepresentation analysis for the genome-wide association study-nominated genes within each cell type cluster yielded no significant results at 5% FDR (Supplementary material, 'Data' section 5).

α-Synuclein pathology is associated with a distinct neuronal gene expression signature

To discern cell-specific changes in gene expression associated with α-synuclein pathology, we compared LRRK2-PD individuals with ($n = 3$, Braak stage 4–5) and without ($n = 4$, Braak stage 0) Lewy pathology. Differential gene expression in each cell type cluster revealed a total of 754 DEGs (henceforth referred to as 'α-synuclein signature'), comprising 589 downregulated and 165 upregulated DEGs. Notably, this was a far larger signal than those observed in the contrasts between diseases and controls (full results are provided in Supplementary material, 'Data' section 6). The α-synuclein signature was predominantly neuronal, with neuronal clusters collectively gathering 647 of 754 DEGs and only 111 of 754 DEGs detected in glial clusters. Furthermore, the largest part of the signal originated from the most abundant types of excitatory neurons, located in the outer cortical layers (ex_01 and ex_02, with 324 and 245 DEGs, respectively) and intermediate layers (ex_06 and ex_11, with 125 and 161 DEGs, respectively; Fig. 6A). This was in sharp contrast to the iPD- and LRRK2-PD-specific transcriptional signatures, where most of the transcriptional dysregulation was observed in deep cortical neurons (clusters ex_19 and ex_24; Fig. 3A and B). In fact, we found that the similarity between Lewy pathology-associated and the disease-specific PD transcriptional signature was low, with only 5% (34 of 647) of neuronal DEGs overlapping with iPD and 1% (6 of 647) with LRRK2-PD (Fig. 6B). The overlap of neuronal Lewy pathology-associated DEGs with MSA was even lower, <1% (4 of 647).

Despite the predominant downregulation signal observed in neurons, α-synuclein pathology was associated with a significant upregulation of the *SNCA* transcript in cluster ex_02 (Fig. 6C). These are excitatory neurons located in the superficial cortical layers (layers 2/3) expressing *CBLN2* and *GNAL* (Fig. 1E). Although ex_02 showed the strongest signal and survived multiple testing correction, the upregulation of *SNCA* was consistent in all excitatory neuronal subtypes and nominally significant in ex_09, ex_17 and ex_19. Notably, altered *SNCA* expression was seen only in the α-synuclein transcriptional signature and not observed in any of the disease-specific contrasts (Fig. 6C). Other noteworthy DEGs associated with α-synuclein pathology included a neuronal upregulation of *HSP90AA1* and *HSP90AB1*, encoding heat shock proteins involved in cellular stress response;[39] *CALM*, encoding calmodulin, an important regulator of calcium signalling; and *OPTN* and *SOD1*, encoding proteins involved in mitophagy and antioxidant response, respectively, mutations in which cause familial amyotrophic lateral sclerosis.[40,41] Additionally, we noted that oligodendrocytes exhibited an upregulation of *VPS13C*, involved in mitochondrial quality control, mutations in which cause recessive parkinsonism with diffuse Lewy body disease[42] (Supplementary material, 'Data' section 6).

Despite the general trend for downregulation, overrepresentation analysis of gene expression associated with α-synuclein pathology in LRRK2-PD individuals unveiled the significant upregulation of processes related to mitochondrial respiration in clusters ex_06 and ex_11 (Supplementary Table 4). This signal was driven by nuclear-encoded components of the respiratory chain. Additionally, we observed an upregulation of the ribosome and protein translation driven by ribosomal proteins, similar to that observed in the iPD- and LRRK2-PD disease-specific signatures, but originating from different neuronal subtypes (i.e. ex_11 and in_12) (Supplementary material, 'Data' section 7).

The common DEGs between the α-synuclein-associated signature in LRRK2-PD individuals and the disease-associated signature in iPD consisted of only 34 neuronal genes, of which 32 were downregulated. Despite not reaching statistical significance in the functional overrepresentation analysis, the downregulated signature was visibly composed of synaptic components (Supplementary material, 'Data' section 8).

Finally, to identify an α-synuclein-associated signature in iPD, we carried out an analogous analysis in the iPD samples. Specifically, we assessed DEGs associated with the severity of Braak stage (range: 4–6). We identified a total of 226 DEGs (140 downregulated and 86 upregulated), whereof the majority (193 of 226) were dysregulated in excitatory neuronal clusters (Supplementary material, 'Data' section 9). Notable among them was an upregulation of *BASP1*, encoding a synaptic protein involved in neurite outgrowth and plasma membrane organization,[43] which was found to be upregulated prominently in induced pluripotent stem cell-derived neurons carrying a pathogenic *SNCA* mutation and expressing α-synuclein pathology.[44]

A total of 37 DEGs were common between the α-synuclein-associated signature in LRRK2-PD and iPD. These included a downregulation, in several excitatory neuronal clusters, of *RPTOR*, encoding a component of the regulatory associated protein of the mammalian target of rapamycin (mTOR) complex 1 (mTORC1), which has a central role in regulating cell metabolism and autophagy.[45] No significant pathway enrichment was found in the overrepresentation analyses.

Discussion

We report cell type-specific changes in gene expression associated with iPD, LRRK2-PD and MSA and with neuronal α-synuclein pathology. Most DEGs in the snRNA-seq dataset (296 of 318) were cell type specific and therefore not identified by bulk RNA-seq in the same samples, highlighting the importance of cell type-specific studies in neurodegeneration.

The transcriptomic signatures of iPD and LRRK2-PD were qualitatively similar, suggesting overlapping disease mechanisms, and highly distinct from that of MSA. Although more genes were significantly differentially expressed in iPD, most of these (201 of 252) were nominally significant in LRRK2-PD, indicating that the difference is mostly attributable to sample size and statistical power.

PD (iPD or LRRK2-PD) exhibited a predominantly neuronal signature, with relatively few DEGs in glia. Strikingly, most of the differential expression signal was concentrated in the excitatory neuronal cluster ex_19. These deep cortical neurons (layers 6/6b), express high levels of the α_{2A}-adrenoreceptor and are therefore likely to receive adrenergic afferents from the noradrenergic neurons of the locus coeruleus,[46] a neuronal population typically degenerated in PD.[47] It is possible that the observed transcriptional dysregulation of these neurons is a result of their adrenergic denervation. This is, however, contradicted by the fact that MSA, which also exhibits degeneration of the locus coeruleus and coeruleocortical afferents,[48,49] does not recapitulate a preferential involvement of the ex_19 neurons.

α_2-Adrenoreceptors are decreased in the PFC of individuals with PD,[50] and α_2-adrenoreceptor agonists have been shown to ameliorate cognitive deficits in patients.[51,52] Interestingly, studies in non-human primates demonstrated that α_2-adrenoreceptor agonists exert these effects by acting mainly on the dorsolateral PFC,[53] the region from which our samples originated. Although the mechanisms underlying the selective involvement of the ex_19 neuronal cluster remain unknown, our findings suggest that aberrant function of these neurons plays a role in iPD and LRRK2-PD. Whether this is related to impaired α_2-adrenergic transmission is unknown, and further research is warranted to understand the involvement of these neurons in PD, in addition to the clinical correlates of their altered function.

Among the DEGs in our dataset, *PDE10A* stood out owing to its strikingly consistent downregulation across nearly all cortical neuronal types in iPD and LRRK2-PD. This observation was confirmed by immunohistochemistry, showing decreased neuronal expression of PDE10A in PD.

PDE10A encodes phosphodiesterase 10A, an enzyme playing an important role in signal transduction by regulating the intracellular levels of cyclic adenosine monophosphate (cAMP) and cyclic guanosine monophosphate (cGMP). PDE10A is highly expressed in human striatal medium spiny neurons, where it is involved in movement control. By hydrolysing cAMP and/or cGMP, PDE10A inhibits dopamine D_1 receptor signalling in the striatonigral pathway and enhances dopamine D_2 receptor signalling in the striatopallidal pathway, thereby leading to an overall decrease of movement.[38,54] Several published cases have demonstrated that mutations in *PDE10A* cause childhood-onset hyperkinetic movement disorders.[55] Using PET, PDE10A has been shown to be decreased in the striatum of PD patients, possibly as a compensatory response to the loss of nigrostriatal dopaminergic input.[38] Moreover, PDE10A inhibitors improve parkinsonistic motor deficits in preclinical animal studies, via their action on the striatal pathways, and have been proposed as a potential dopamine-independent motor treatment for PD.[54,56] However, the physiological function and disease relevance of PDE10A outside the striatum are unknown.

We show that PDE10A mRNA and protein are highly expressed in neurons and endothelial cells of the human PFC. Moreover, PDE10A expression is dysregulated across most neuronal types of the PFC in iPD and LRRK2-PD, indicating that the implication of this protein in the pathogenesis of PD extends well beyond regulation of dopaminergic transmission in the striatum and motor control. It is possible that the altered PDE10A expression in the PFC is involved in altered transmission within that region, contributing to non-motor dysfunction in PD, including cognitive and emotional dysregulation. Further investigation into the functional implications of PDE10A dysregulation in the PD cortex could provide valuable insights into molecular disease mechanisms and potential therapeutic targets.

The cell-specific transcriptomic signature of MSA was highly distinct from that of PD, in terms of both dysregulated genes and affected cell types. In addition to multiple DEGs in neurons, MSA exhibited a prominent oligodendroglial signal, in line with its glial pathology.[1,2] Moreover, MSA showed no predilection for the ex_19 neuronal cluster and no significant dysregulation of the *PDE10A* gene.

In all three diseases, the number of glial DEGs was notably smaller compared with that of neurons. Regardless of disease status, glia expressed on average 50% fewer genes than neurons and exhibited a lower average gene expression, including housekeeping genes. This might simply reflect structural and functional differences between cell types, such as the overall smaller size (i.e. cytoplasmic volume) and lower metabolic activity of glia compared with neurons.[23,57,58] Such differences in transcriptional volume could result in lower coverage of glial transcripts, with a lower power of discovery. Higher sequencing depths or resorting to cell enrichment techniques might yield a more detailed characterization of the transcriptional landscape of glial cell populations.

Harnessing the variable presence of α-synuclein pathology in LRRK2-PD allowed us to discern cell-specific transcriptomic signatures associated with α-synuclein pathology. Strikingly, this comprised a neuronal upregulation of the *SNCA* gene itself, in addition to several genes involved in stress response to oxidative damage, calcium regulation and mitochondrial function. At the pathway level, α-synuclein pathology was strongly associated with an upregulation of processes involved in mitochondrial respiration, including components of the respiratory chain itself. This phenomenon might represent a compensatory response to respiratory dysfunction, which has been shown to be associated with early forms of α-synuclein pathology in PD neurons.[59] However, whether this is relevant for LRRK2 disease is currently unknown.

iPD exhibited a generally weaker α-synuclein-associated signature compared with LRRK2-PD. This could be because, unlike LRRK2-PD, all iPD individuals in our study harboured α-synuclein pathology (Braak stage 4–6), leading to less variability and contrast compared with LRRK2-PD (Braak stage 0–5). Ideally, this should be studied across a wider range of α-synuclein pathology, but brain tissue from individuals with early-stage iPD was not available to us. Thus, we believe that the analysis of LRRK2-PD is more sensitive and specific in this regard, and differential expression signatures should not be considered less relevant for not being present also in iPD. Nevertheless, altered expression in some genes was found to be associated with α-synuclein pathology in both LRRK2-PD and iPD, including neuronal downregulation of *RPTOR*. This finding suggests that a dysregulation of the mTORC1 pathway, which has a central role in regulating cell metabolism and autophagy,[45] might be involved in the pathogenesis of α-synucleinopathies. Aberrant mTOR/mTORC1 signalling has also been found in preclinical models of PD.[60] Moreover, mTOR/mTORC1 signalling can be modulated by a number of approved drugs, including the glucagon-like peptide 1 (GLP-1) receptor agonist exenatide, which are currently in trials for iPD, with encouraging results so far.[61]

Another noteworthy observation is that in iPD, the severity of α-synuclein pathology was associated with upregulation of *BASP1*.

This gene encodes a synaptic protein involved in neurite outgrowth and plasma membrane organization[43] and was found to be upregulated in induced pluripotent stem cell-derived neurons carrying a pathogenic *SNCA* mutation and expressing α-synuclein pathology.[44] Our findings indicate that *BASP1* dysregulation is associated with α-synuclein pathology in the brain of patients with iPD.

Finally, in addition to altered expression in specific genes and pathways, we identify a general trend for a disease-specific reduction in the overall neuronal transcriptional output. This intriguing phenomenon, which might reflect a general metabolic decline in dysfunctional neurons, was more pronounced in inhibitory neurons and not encountered in glial cells. Inhibitory neurons might indeed be more vulnerable owing to their higher metabolic requirements.[62] Regardless of its biological significance, this phenomenon explains the observed discrepancy between bulk RNA-seq, indicating a decrease in the neuronal fraction and an increase in glial populations, and snRNA-seq data, which indicated no change in cell composition. This has important methodological implications for the field of brain omics. Given that current methods for estimating cell composition in bulk brain tissue transcriptomic data are based on the expression of cell type markers, they cannot distinguish between a reduction in the number of cells and the transcriptional output of a particular cell type. Thus, bulk tissue transcriptomics-based reports of neuronal loss in PD might be driven, at least in part, by a reduction in overall neuronal transcriptional output. Another possible explanation might be the loss of synaptic input to the PFC from deeper regions, including the basal forebrain nuclei and locus coeruleus, which characterizes α-synucleinopathies. Given that synapses also contain neuronal RNA, they contribute to the cell proportion estimates in bulk tissue but do not influence snRNA data. These findings raise questions about the validity of using bulk RNA-seq data to assess cellular composition in complex neurodegenerative diseases and emphasize the importance of single-cell analyses to gain a more accurate understanding of cell type-specific changes.

Data availability

The code required to reproduce the results of these analyses is available in the Neuromics Group Gitlab repository, https://git.app.uib.no/neuromics/sn-rna-seq-alphasyn. The raw datasets generated in this study are available in the EGA repository (dataset accession numbers EGAD50000000430 and EGAD50000000431).

Acknowledgements

We are deeply grateful to the study participants and their families involved in the study for their unique contribution. Furthermore, we would like to thank the entire Park West study consortium for their diligent efforts in characterizing and following the Park West cohort; the Neurological Tissue Bank of the IDIBAPS-Hospital Clinic for providing data and samples; the Netherlands Brain Bank; the London Neurodegenerative Diseases Brain Bank; Dr Romain Guitton, Dr Kristoffer Haugarvoll and Janani Sundaresan for helping to dissect and prepare the brain tissue; and Gry Hilde Nilsen for technical support.

Funding

This work is supported by grants from The Research Council of Norway (288164) and Stiftelsen Kristian Gerhard Jebsen (SKGJ-MED-023).

Competing interests

The authors report no competing interests.

Supplementary material

Supplementary material is available at *Brain* online.

References

1. Koga S, Sekiya H, Kondru N, Ross OA, Dickson DW. Neuropathology and molecular diagnosis of synucleinopathies. *Mol Neurodegener*. 2021;16:83.
2. Galvin JE, Lee VMY, Trojanowski JQ. Synucleinopathies: Clinical and pathological implications. *Arch Neurol*. 2001;58:186-190.
3. Dickson DW. Parkinson's disease and parkinsonism: Neuropathology. *Cold Spring Harb Perspect Med*. 2012;2:a009258.
4. Fanciulli A, Wenning GK. Multiple-system atrophy. *N Engl J Med*. 2015;372:249-263.
5. Ahmed Z, Asi YT, Sailer A, et al. The neuropathology, pathophysiology and genetics of multiple system atrophy. *Neuropathol Appl Neurobiol*. 2012;38:4-24.
6. Henderson MX, Sengupta M, Trojanowski JQ, Lee VMY. Alzheimer's disease tau is a prominent pathology in LRRK2 Parkinson's disease. *Acta Neuropathol Commun*. 2019;7:183.
7. Kalia LV, Lang AE, Hazrati LN, et al. Clinical correlations with Lewy body pathology in LRRK2-related Parkinson disease. *JAMA Neurol*. 2015;72:100-105.
8. Nido GS, Dick F, Toker L, et al. Common gene expression signatures in Parkinson's disease are driven by changes in cell composition. *Acta Neuropathol Commun*. 2020;8:55.
9. Toker L, Nido GS, Tzoulis C. Not every estimate counts – evaluation of cell composition estimation approaches in brain bulk tissue data. *Genome Med*. 2023;15:41.
10. Dick F, Johanson GS, Tzoulis C. Neuronal loss drives differentially expressed protein-pathways in the PSP globus pallidus. *Clin Transl Med*. 2023;13:e1280.
11. Smajić S, Prada-Medina CA, Landoulsi Z, et al. Single-cell sequencing of human midbrain reveals glial activation and a Parkinson-specific neuronal state. *Brain*. 2022;145:964-978.
12. Kamath T, Abdulraouf A, Burris SJ, et al. Single-cell genomic profiling of human dopamine neurons identifies a population that selectively degenerates in Parkinson's disease. *Nat Neurosci*. 2022;25:588-595.
13. Zarow C, Lyness SA, Mortimer JA, Chui HC. Neuronal loss is greater in the locus coeruleus than nucleus basalis and substantia nigra in Alzheimer and Parkinson diseases. *Arch Neurol*. 2003;60:337-341.
14. Alves G, Müller B, Herlofson K, et al. Incidence of Parkinson's disease in Norway: The Norwegian ParkWest study. *J Neurol Neurosurg Psychiatry*. 2009;80:851-857.
15. Kim D, Langmead B, Salzberg SL. HISAT: A fast spliced aligner with low memory requirements. *Nat Methods*. 2015;12:357-360.
16. Van der Auwera GA, Carneiro MO, Hartl C, et al. From FastQ data to high-confidence variant calls: The genome analysis toolkit best practices pipeline. *Curr Protoc Bioinforma*. 2013;43:11.10.1-11.10.33.
17. Gelb DJ, Oliver E, Gilman S. Diagnostic criteria for Parkinson disease. *Arch Neurol*. 1999;56:33-39.
18. Ward CD. Research diagnostic criteria for Parkinson's disease. *Adv Neurol*. 1990;53:245-249.
19. Lee H, Fenster RJ, Pineda SS, et al. Cell type-specific transcriptomics reveals that mutant huntingtin leads to mitochondrial

RNA release and neuronal innate immune activation. *Neuron*. 2020;107:891-908.e8.
20. Caglayan E, Liu Y, Konopka G. Neuronal ambient RNA contamination causes misinterpreted and masked cell types in brain single-nuclei datasets. *Neuron*. 2022;110:4043-4056.e5.
21. Fleming SJ, Chaffin MD, Arduini A, et al. Unsupervised removal of systematic background noise from droplet-based single-cell experiments using CellBender. *Nat Methods*. 2023; 20:1323-1335.
22. McGinnis CS, Murrow LM, Gartner ZJ. DoubletFinder: Doublet detection in single-cell RNA sequencing data using artificial nearest neighbors. *Cell Syst*. 2019;8:329-337.e4.
23. Magistretti PJ, Allaman I. A cellular perspective on brain energy metabolism and functional imaging. *Neuron*. 2015;86:883-901.
24. Lake BB, Ai R, Kaeser GE, et al. Neuronal subtypes and diversity revealed by single-nucleus RNA sequencing of the human brain. *Science*. 2016;352:1586-1590.
25. Patro R, Duggal G, Love MI, Irizarry RA, Kingsford C. Salmon provides fast and bias-aware quantification of transcript expression. *Nat Methods*. 2017;14:417-419.
26. Soneson C, Love MI, Robinson MD. Differential analyses for RNA-seq: Transcript-level estimates improve gene-level inferences. *F1000Res*. 2015;4:1521.
27. Mancarci BO, Toker L, Tripathy SJ, et al. Cross-laboratory analysis of brain cell type transcriptomes with applications to interpretation of bulk tissue data. *Eneuro*. 2017;4: ENEURO.0212-17.2017.
28. Love MI, Huber W, Anders S. Moderated estimation of fold change and dispersion for RNA-seq data with DESeq2. *Genome Biol*. 2014;15:550.
29. Mancarci O. Homologene: Quick Access to Homologene and Gene Annotation Updates. R package version 1.4.68.19.3.27. Comprehensive R Archive Network (CRAN). https://CRAN.R-project.org/package=homologene
30. Dachet F, Brown JB, Valyi-Nagy T, et al. Selective time-dependent changes in activity and cell-specific gene expression in human postmortem brain. *Sci Reports*. 2021;11:6078.
31. Finak G, McDavid A, Yajima M, et al. MAST: A flexible statistical framework for assessing transcriptional changes and characterizing heterogeneity in single-cell RNA sequencing data. *Genome Biol*. 2015;16:278.
32. Nalls MA, Blauwendraat C, Vallerga CL, et al. Identification of novel risk loci, causal insights, and heritable risk for Parkinson's disease: A meta-analysis of genome-wide association studies. *Lancet Neurol*. 2019;18:1091-1102.
33. Korotkevich G, Sukhov V, Budin N, Shpak B, Artyomov MN, Sergushichev A. Fast gene set enrichment analysis. *bioRxiv*. [Preprint]. https://doi.org/10.1101/060012
34. Kuleshov MV, Jones MR, Rouillard AD, et al. Enrichr: A comprehensive gene set enrichment analysis web server 2016 update. *Nucleic Acids Res*. 2016;44(Web Server issue):W90-W97.
35. Subramanian A, Tamayo P, Mootha VK, et al. Gene set enrichment analysis: A knowledge-based approach for interpreting genome-wide expression profiles. *Proc Natl Acad Sci U S A*. 2005;102:15545-15550.
36. Liberzon A, Birger C, Thorvaldsdóttir H, Ghandi M, Mesirov JP, Tamayo P. The molecular signatures database hallmark gene set collection. *Cell Syst*. 2015;1:417-425.
37. Thrupp N, Sala Frigerio C, Wolfs L, et al. Single-nucleus RNA-Seq is not suitable for detection of microglial activation genes in humans. *Cell Rep*. 2020;32:108189.
38. Erro R, Mencacci NE, Bhatia KP. The emerging role of phosphodiesterases in movement disorders. *Mov Disord*. 2021;36: 2225-2243.
39. Zuehlke AD, Beebe K, Neckers L, Prince T. Regulation and function of the human *HSP90AA1* gene. *Gene*. 2015;570:8-16.
40. Lazarou M, Sliter DA, Kane LA, et al. The ubiquitin kinase PINK1 recruits autophagy receptors to induce mitophagy. *Nature*. 2015; 524:309-314.
41. Trist BG, Hilton JB, Hare DJ, Crouch PJ, Double KL. Superoxide dismutase 1 in health and disease: How a frontline antioxidant becomes neurotoxic. *Angew Chem Int Ed Engl*. 2021;60:9215-9246.
42. Lesage S, Drouet V, Majounie E, et al. Loss of VPS13C function in autosomal-recessive parkinsonism causes mitochondrial dysfunction and increases PINK1/Parkin-dependent mitophagy. *Am J Hum Genet*. 2016;98:500-513.
43. Korshunova I, Caroni P, Kolkova K, Berezin V, Bock E, Walmod PS. Characterization of BASP1-mediated neurite outgrowth. *J Neurosci Res*. 2008;86:2201-2213.
44. Fernandes HJR, Patikas N, Foskolou S, et al. Single-cell transcriptomics of Parkinson's disease human *in vitro* models reveals dopamine neuron-specific stress responses. *Cell Rep*. 2020;33: 108263.
45. Foster KG, Acosta-Jaquez HA, Romeo Y, et al. Regulation of mTOR complex 1 (mTORC1) by raptor Ser863 and multisite phosphorylation. *J Biol Chem*. 2010;285:80-94.
46. Samuels E, Szabadi E. Functional neuroanatomy of the noradrenergic locus coeruleus: Its roles in the regulation of arousal and autonomic function part I: Principles of functional organisation. *Curr Neuropharmacol*. 2008;6:235-253.
47. Dickson DW. Neuropathology of Parkinson disease. *Park Relat Disord*. 2018;46:S30-S33.
48. Benarroch EE, Schmeichel AM, Low PA, Sandroni P, Parisi JE. Loss of A5 noradrenergic neurons in multiple system atrophy. *Acta Neuropathol*. 2008;115:629-634.
49. Betts MJ, Kirilina E, Otaduy MCG, et al. Locus coeruleus imaging as a biomarker for noradrenergic dysfunction in neurodegenerative diseases. *Brain*. 2019;142:2558-2571.
50. Cash R, Ruberg M, Raisman R, Agid Y. Adrenergic receptors in Parkinson's disease. *Brain Res*. 1984;322:269-275.
51. Jäkälä P, Riekkinen M, Sirviö J, et al. Guanfacine, but not clonidine, improves planning and working memory performance in humans. *Neuropsychopharmacology*. 1999;20:460-470.
52. Riekkinen M, Riekkinen P. α_2-Adrenergic agonist clonidine for improving spatial working memory in Parkinson's disease. *J Clin Psychopharmacol*. 1999;19:444-449.
53. Arnsten AFT, Goldman-Rakic PS. α_2-Adrenergic mechanisms in prefrontal cortex associated with cognitive decline in aged nonhuman primates. *Science*. 1985;230:1273-1276.
54. Sukhanov I, Dorotenko A, Fesenko Z, et al. Inhibition of PDE10A in a new rat model of severe dopamine depletion suggests new approach to non-dopamine Parkinson's disease therapy. *Biomolecules*. 2022;13:9.
55. Kalampokini S, Xiromerisiou G, Bargiotas P, Anastasiadou VC, Costeas P, Hadjigeorgiou GM. PDE10A mutation as an emerging cause of childhood-onset hyperkinetic movement disorders: A review of all published cases. *Neuropediatrics*. 2024;55:217-223.
56. Lenda T, Ossowska K, Berghauzen-Maciejewska K, et al. Antiparkinsonian-like effects of CPL500036, a novel selective inhibitor of phosphodiesterase 10A, in the unilateral rat model of Parkinson's disease. *Eur J Pharmacol*. 2021;910:174460.
57. Harris JJ, Jolivet R, Attwell D. Synaptic energy use and supply. *Neuron*. 2012;75:762-777.
58. Hyder F, Rothman DL, Bennett MR. Cortical energy demands of signaling and nonsignaling components in brain are conserved across mammalian species and activity levels. *Proc Natl Acad Sci U S A*. 2013;110:3549-3554.

59. Flønes IH, Nyland H, Sandnes DA, Alves GW, Tysnes OB, Tzoulis C. Early forms of α-synuclein pathology are associated with neuronal complex I deficiency in the substantia nigra of individuals with Parkinson's disease. *Biomolecules*. 2022;12:747.
60. Kosillo P, Ahmed KM, Aisenberg EE, et al. Dopamine neuron morphology and output are differentially controlled by mTORC1 and mTORC2. *Elife*. 2022;11:e75398.
61. Athauda D, Maclagan K, Skene SS, et al. Exenatide once weekly versus placebo in Parkinson's disease: A randomised, double-blind, placebo-controlled trial. *Lancet*. 2017; 390:1664-1675.
62. Lax NZ, Grady J, Laude A, et al. Extensive respiratory chain defects in inhibitory interneurones in patients with mitochondrial disease. *Neuropathol Appl Neurobiol*. 2016;42:180-193.